Supplementary Information from the article "Free-atom-like d-states in single atom alloy catalysts"

M. T. Greiner, T. E. Jones, S. Beeg, L. Zwiener, M. Scherzer, F. Girgsdies, S. Piccinin, M. Armbrüster, A. Knop-Gericke, R. Schlögl

Contents

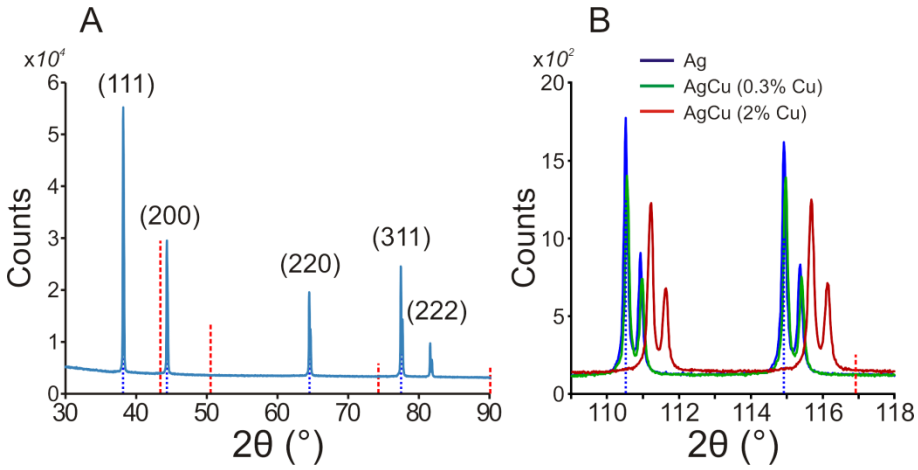

Figure 1 - A) X-ray powder diffraction pattern of AgCu (0.3 at. % Cu), showing the expected positions of pure Ag (dotted line) and pure Cu (dashed line). B) High-angle diffraction pattern of pure Ag, AgCu (0.3 at. % Cu) and AgCu (2 at. % Cu). This data shows that the synthesized AgCu alloys were single phase (no detectible phase segregation) and that the presence of Cu in the Ag lattice gives rise to an expected lattice contraction.

Silver and copper have a rather limited range of solubility,[4] with a solubility of Cu in Ag at room temperature of only ca. 0.5 atomic percent, and higher concentrations giving rise to phase segregation. In order to verify that the alloys we were analyzing were phase pure, we performed XRD measurements to look for evidence of Cu lattice reflections. As one cans see in Figure 1, the alloy was phase pure, with diffraction lines resembling a slightly contracted Ag lattice.

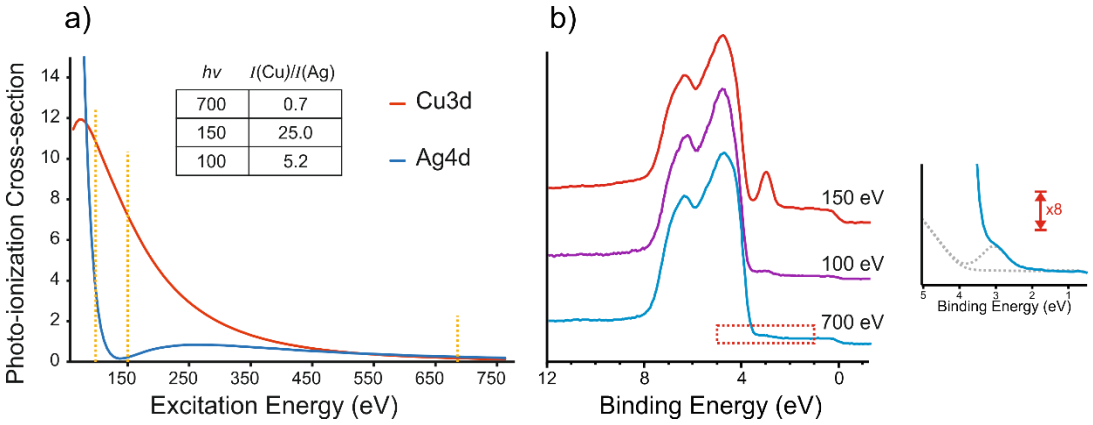

Figure 2 - a) Calculated photo-ionization cross sections of the Ag4d and Cu3d states. The dashed vertical lines indicate the photon energies used in this work. The table inset shows the ratio of Cu3d to Ag4d photoemission intensity at the respective photon energies. b) Valence band photoemission spectra of reduce AgCu (0.5 At. % Cu) at the three photon energies highlighted by vertical lines in part a). The inset shows a magnified vies of the Cu3d states when measured using 700 eV photons. The peak with is the same as when measured at the Cooper minimum, but the intensity is greatly decreased relative to the Ag4d states.

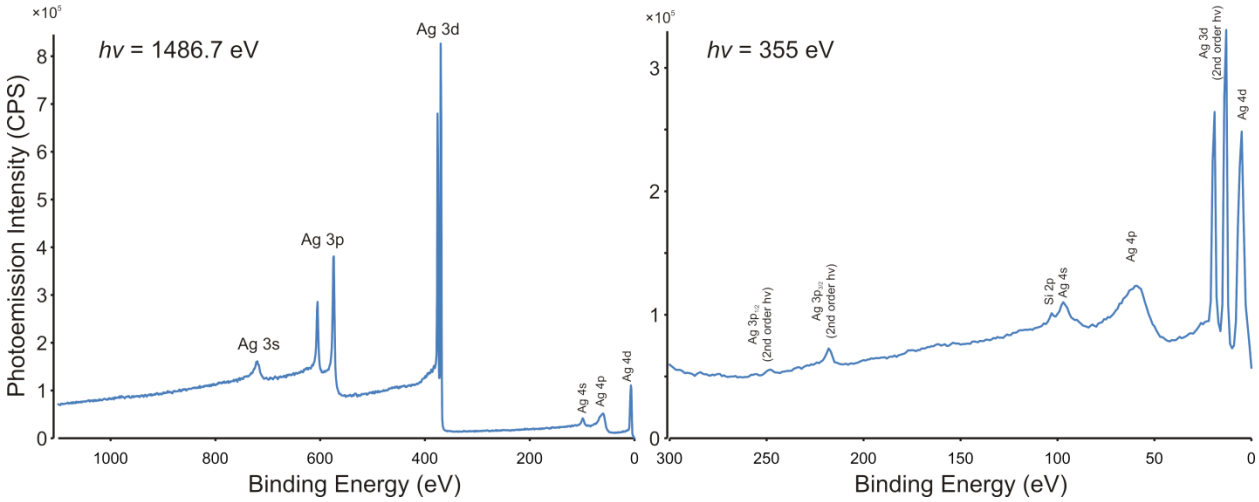

Figure 3 - Survey spectra of sputter cleaned and reduced AgCu alloy (0.3 at. % Cu). The spectrum on the left was measured with a photon energy of 1486.7 eV for comparison with laboratory source XPS. The spectrum on the right was measured with a photon energy of 355 eV for high sensitivity to low atomic weight elements, such as common impurities like C, Li, K, Si, F, S, etc. One can see that the alloy is rather clean, with no detectible C or O and a negligible amount of Si. Note the appearance of photoemission peaks from photoelectrons generated from the second order diffraction of the monochromated photons.

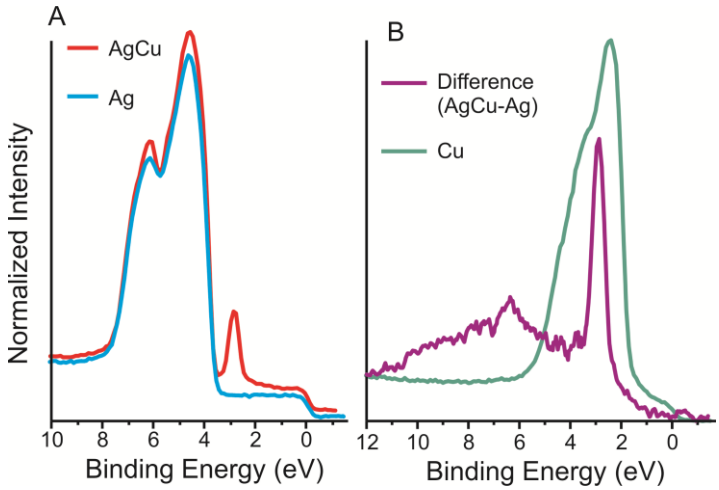

Figure4 - Valence band photoemission spectra (hv = 150 eV) of 0.3 at. % AgCu and pure Ag (left), and the difference of AgCu-Ag overlaid on a spectrum of pure Cu. The comparison of the difference spectrum with the spectrum of bulk Cu clearly demonstrates the stark contrast between pure Cu and Cu ions in AgCu. The FWHM of the Cu3d band in pure Cu is ca. 2.5 eV, while in AgCu it is 0.5 eV.

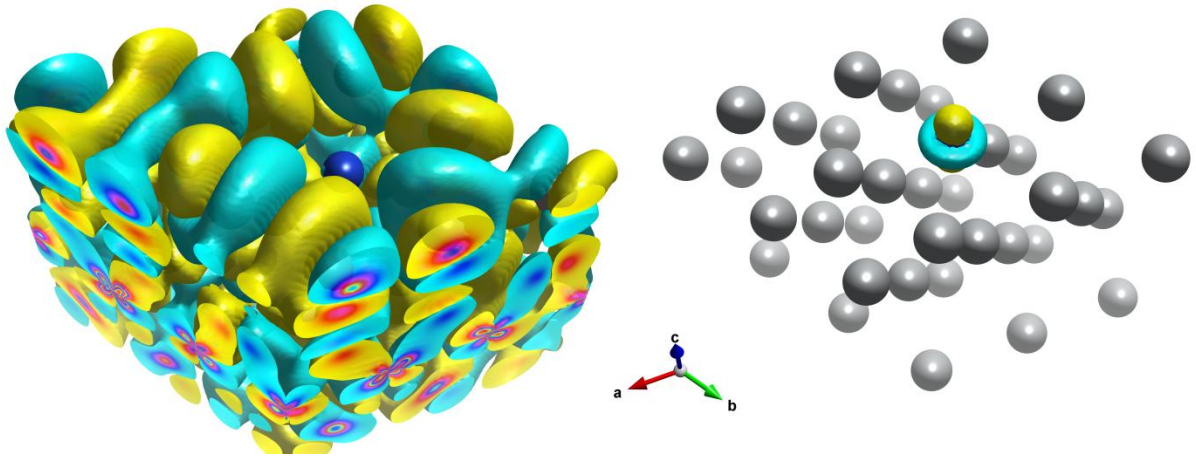

Figure 5 - Comparison of the spatial extent of a Ag4d wavefunction in $Ag_{35}Cu_1$ with a Cu3d wavefunction. On the left, one can see that the Ag4d wavefunction is delocalized across the entire lattice (except where the Cu ions sit). The figure on the right demonstrates how localized the Cu3d states are. Their spatial extent is restricted to being localized on the Cu ions.

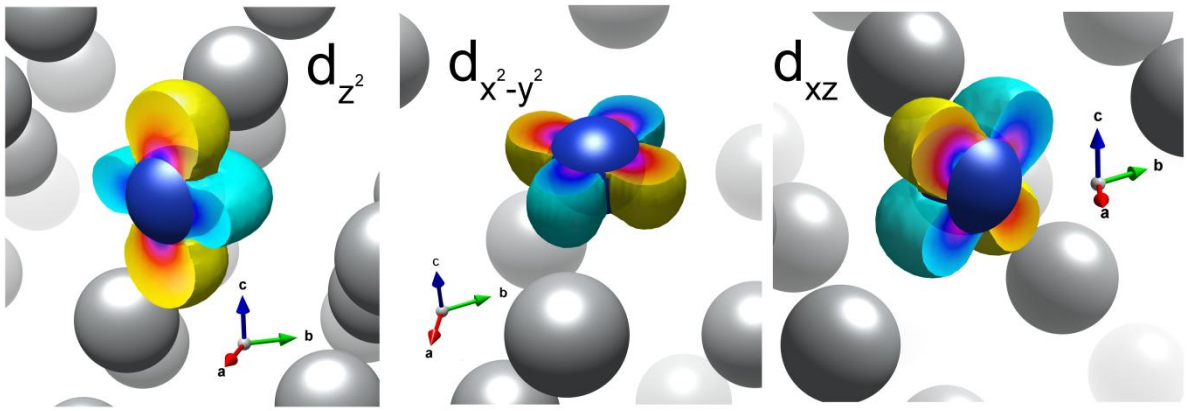

Figure 6 - Calculated Cu 3d wavefunctions of $Ag_{35}Cu_1$. These wavefunctions represent the states at ca. 2.0 eV in the pDOS shown in Figure 1 of the main text. Note the free-atom-like nature of these states.

In order to test whether the narrow d-band of Cu is a result of poor spatial overlap with Ag ions, we performed a theory experiment whereby we compressed the lattice of the AgCu alloy such that it has the same lattice spacing as pure Cu. The pDOS calculations shown in Figure 7 reveal that the lattice constant has only a minimal influence on the Cu3d bandwidth. Compressing the lattice mainly shifts the Cu3d band toward higher binding energy, but the bandwidth stays essentially the same. The symmetry-resolved pDOS of the Cu3d states shown in Figure 7 b) show that the t_{2g} and e_g states remain nearly degenerate in the compressed lattice. Figure 7 c) shows that even with the shift Cu3d band in the compressed lattice, there is still minimal energy overlap between the Cu3d and Ag4d states.

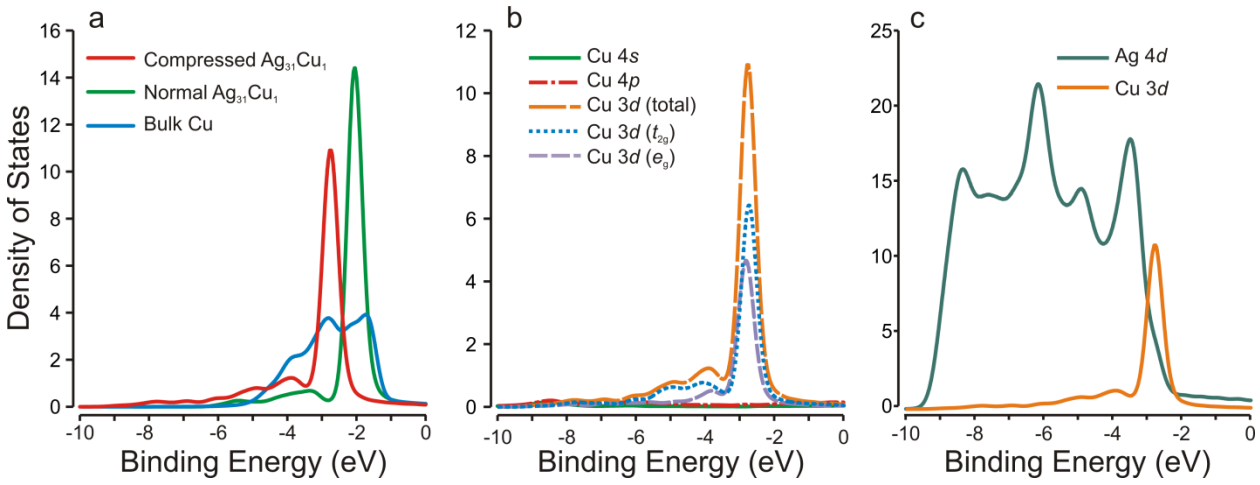

Figure 7 - A) Comparison of Cu 3d pDOS for bulk Cu, $Ag_{31}Cu_1$ with it equilibrium lattice spacing, and $Ag_{31}Cu_1$ with a compressed lattice. B) Cu pDOS of Cu atoms in the compressed $Ag_{31}Cu_1$ lattice. C) Cu 3d pDOS and Ag 4d pDOS of the Ag atoms directly bonded to Cu in compressed $Ag_{31}Cu_1$.

To understand the qualitative features of the Cu *L*-edge NEXAFS spectra, we have calculated symmetry resolved pDOS of the unoccupied Cu states. These are shown in Figure 8 (left). One can see here that the two peaks in the Cu *L*-edge spectra represent hybridizations between Cu4*s* and Cu3*d* states. The first peak represents an unoccupied state that is a hybridization between Cu4*s* states and 3*d* states of t_{2g} symmetry, while the second peak represents unoccupied states from a hybridization between Cu4*s* and 3*d* states of e_g symmetry. Cu L-edge spectra (Figure 8 (right)) were calculated with and without considering p→s transitions by way of the projector augmented wave formalism developed in [O. Bunau and M. Calandra, Phys. Rev. B 87, 205105 (2013)]. Calculations were performed with the Xspectra package [Ch. Gougoussis, M. Calandra, A. P. Seitsonen, F. Mauri, Phys. Rev. B 80, 075102 (2009); M. Taillefumier, D. Cabaret, A. M. Flank, and F. Mauri, Phys. Rev. B 66, 195107 (2002)] using a 20×20×20 k-point mesh. The ground state was calculated using an ultrasoft pseudopotential with three projectors for the l=2 channel and one for the l=0 channel with a kinetic energy (charge density) cutoff of 60 Ry (600 Ry) and a 20×20×20 k-point mesh. Other numerical parameters match those used throughout the main text.

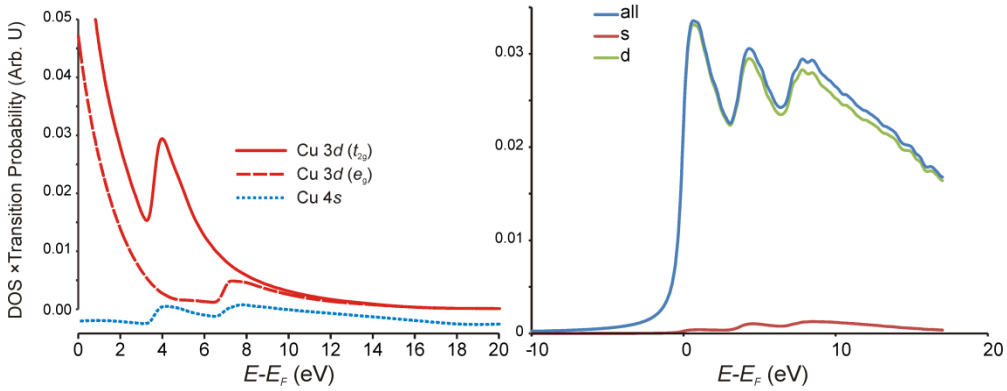

Figure 8 - (left) Computed partial density of unoccupied states (scaled by the transition probability from $2p_{3/2}$ states into the unoccupied states according to Ebert et. al., Phys. Rev. B, v53(23), 16067, 1996) for bulk Cu. (right) calculated Cu L_3-edge NEXAFS spectrum, showing contributions from transitions into d states and s states.

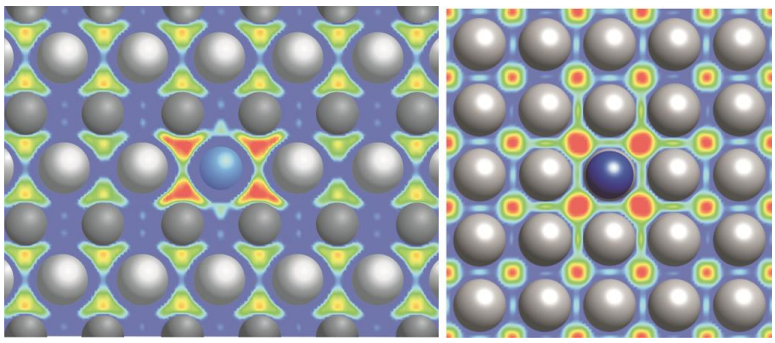

Figure 9 - Computed charge density difference plots along the (110) and (100) planes in $Ag_{31}Cu_1$.

The increased charge density around the Cu ion can be seen using charge-density difference plots. Here we have subtracted from the computed charge density of the alloy, the charge density of the respective free atoms. The intensity centered around the Cu ion indicates that it has a higher charge density than it would as a free atom. It is interesting to note that the symmetry of the additional charge density is e_g.

Table 1 - Voronoi and Löwdin electron population analysis. The *s*, *p* and *d* populations are from the Löwdin analysis. These results show that using both integration methods, the electron count on the Cu ions is higher in AgCu than in elemental Cu. Voronoi charge integration was computed according to [Guerra, Handgraaf, Baerends, Bickelhaupt, *Computational Chemistry*, 25, (2004) 189]. Löwdin charge integration was computed according to [Löwdin, J. Chem. Phys. 18 (1950) 365].

	Electron Count (Voronoi)	Electron Count (Löwdin)	*s*	*p*	*d*
Cu in bulk Cu	11.0	10.9926	0.3527	0.9511	9.6889
Cu in $Ag_{31}Cu_1$	11.4	11.1243	0.4001	0.9751	9.7492
delta	0.4	0.1317	0.0474	0.024	0.0603

Table 2 shows that the direction of chare transfer (i.e. from Ag to Cu) is the same regardless of whether it is a Cu ion in an Ag lattice or an Ag ion in a Cu lattice. Furthermore, it shows that the charge on the Cu ion in the AgCu lattice does not increase with increasing unit cell size.

Table 2 - Voronoi charges and solute-solvent bond lengths for various AgCu compositions.

Material	**Solute Atom**	**Solvent Atom**	**Solute Electron Count (*e*)**	**Δ Solute Charge (*e*)**	**Solvent Electron Count (*e*)**	**Solute-Solvent Bond Length (Å)**	**Lattice Constant (Å)**
Cu	Cu	Cu	11.0	0	11.0	2.59	3.67
$Cu_{31}Ag_1$	Ag	Cu	10.8	+0.2	11.0	2.62	3.63
$Ag_{31}Cu_1$	Cu	Ag	11.4	-0.4	11.0	2.89	4.12
$Ag_{107}Cu_1$	Cu	Ag	11.4	-0.4	11.0	2.89	4.15
Ag	Ag	Ag	11.0	0	11.0	2.94	4.15

In order to examine how Cu-Cu bonding affects the Cu 3d bandwidth, we calculated the pDOS of AgCu slabs containing one to seven Cu ions, where in the cases where more than one Cu ion is present, the Cu ions are nearest neighbors. The geometries are shown in Figure 10 (a) and the calculated Cu3d pDOS are shown in 10 (b). Here one sees that the d-states lose their degeneracy as the number of Cu-Cu bonds increases. Figure 10 (c) and (d) show symmetry-resolved Cu 3d pDOS of AgCu2 and AgCu7. From 10 (c) it is clear that the d-state degeneracy is lost upon the formation of one Cu-Cu bond (as seen by the splitting of the d_{x2-y2} state). When the coordination ring around the central Cu atom is fully occupied (i.e. AgCu7) there is strong splitting of all d-states.

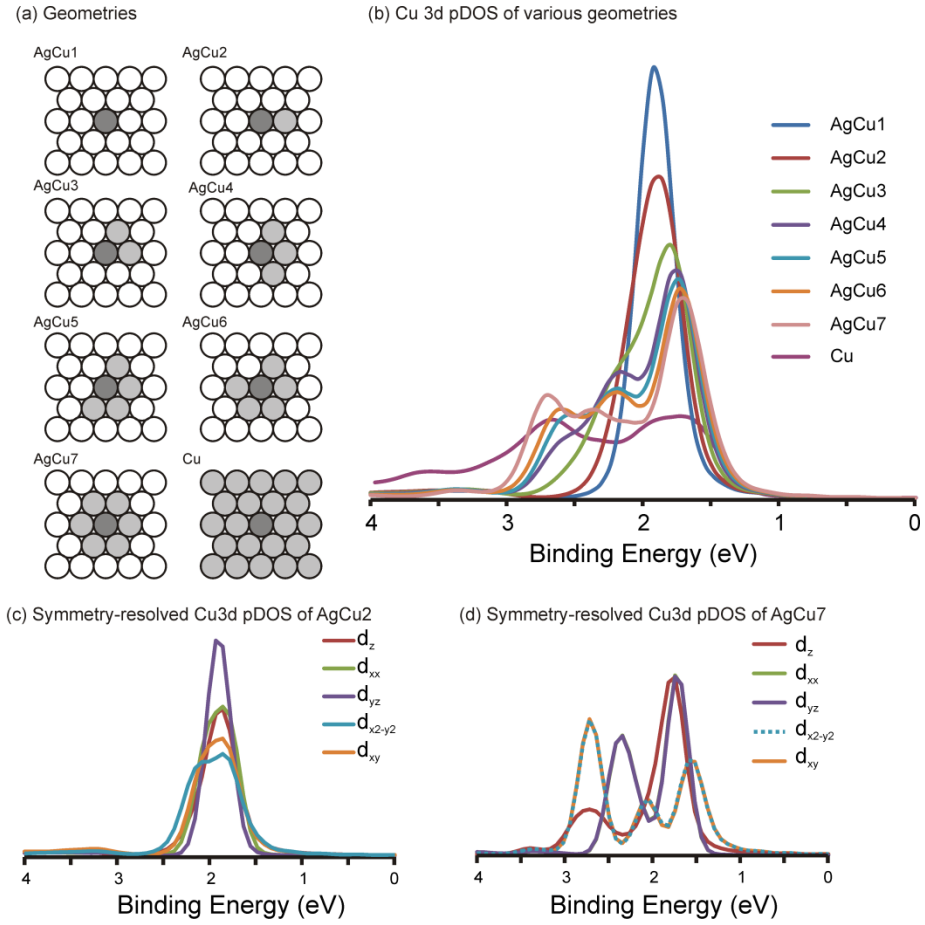

Figure 10 – (a) Geometries for AgCu surface alloys with increasing number of Cu-Cu bonds. (b) Calculated Cu3d pDOS of AgCu alloys of various Cu content, where the number of Cu-Cu bonds progressively increase. These results show that the Cu3d band increases with increasing number of Cu-Cu bonds. The narrowest band is found for the single Cu atom, and the band becomes split when Cu-Cu bonds form. (c) Symmetry-resolved Cu3d pDOS of the case where only one Cu-Cu bond forms, showing splitting of the d_{x2-y2} state. (d) Symmetry resolved Cu3d pDOS of the case where the first coordination ring around the central Cu atom is occupied by other Cu atoms, showing splitting of all Cu d-states.

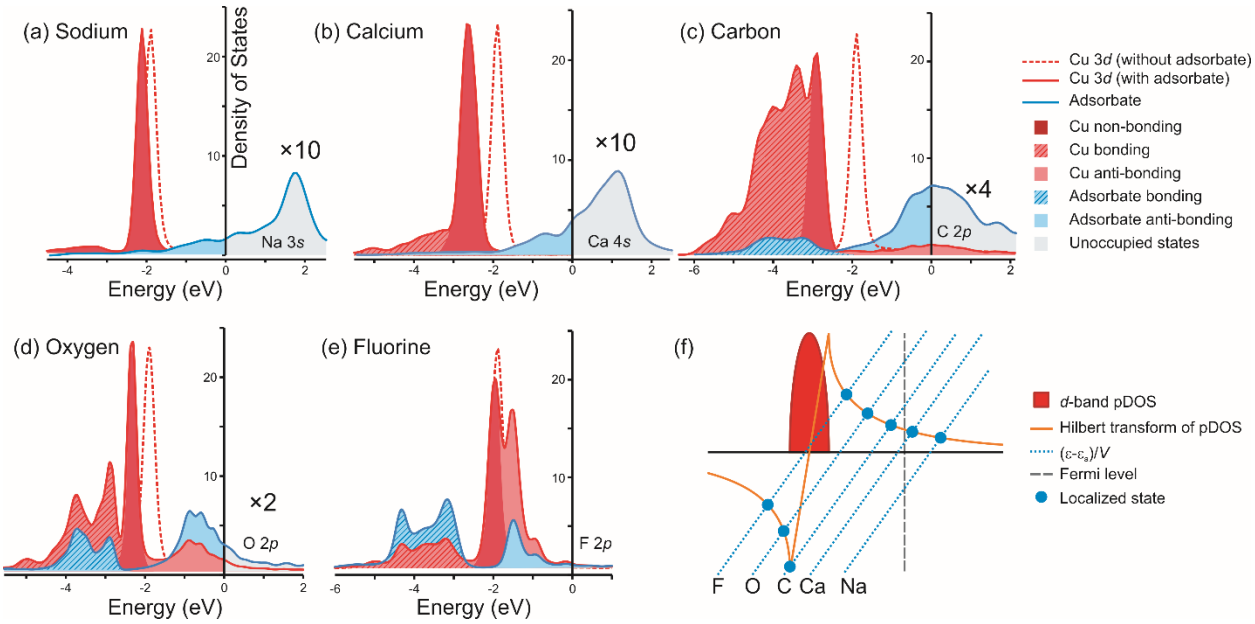

Figure 11 - (a)-(e) pDOS plots of representative adsorbates from each group of the periodic table presented in figure 4. Other adsorbates from the respective groups have qualitatively similar pDOS (see SI). The dashed red curve indicates the unperturbed Cu 3d band, the solid red curve represents the Cu 3d band after interaction with the respective adsorbates. The blue curve represents the pDOS of the respective adsorbate valence states. The solid red filling indicates Cu d-states that do not hybridize with the adsorbates. The hatched regions indicate the bonding states, and the non-hatched regions indicate anti-bonding states. The light blue filling above the Fermi level indicates empty states. (f) shows a graphical solution to the Newns-Anderson model, illustrating how the pDOS's of (a)-(e) arise from the interaction between adsorbate states and the Cu 3d-band.

The following discussion explains the covalent bonding contribution to the periodic trends in Figure 5 (in the main text) using calculated pDOS and the Newns-Anderson-Grimley model. The groups can be classified according to the kind of covalent interaction they have with the substrate. In Figure 11 a)-e) we show pDOS's of representative adsorbates from each group. The Newns-Anderson-Grimley model of adsorbate bonding was found to be an extremely useful and simple graphical means of understanding these covalent bonding trends.

Here we draw comparisons between the Newns-Anderson-Grimley solution and the calculated pDOS's of the adsorbed adsorbates on AgCu in Figure 11 a)-e). The $(\varepsilon-\varepsilon_a)/V^2$ lines for each group of adsorbates are schematically represented in Figure 11 f). For simplicity we have plotted these lines with identical slopes, but this is not generally the case. V determines the slope of the adsorption function, and the overlap integral (V) generally differs among adsorbates. From groups 1-7 the ε_a value decrease. For Na and the group 1 adsorbates, ε_a sits above the Fermi level, and intersects the Hilbert transform only once. This represents a weak interaction with the *d*-band and gives rise to a weakly interacting Na 2*s* state that is mostly unoccupied and can be described as an ionic bond. In the calculated pDOS of Figure 11 a) one can see that the Na 2*s* band is a broad feature that sits mainly above the Fermi level, and the Cu 3*d* band in the alloy exhibits no signs of re-hybridization. When compared with the unperturbed Cu 3*d* state of the alloy (as shown by the dashed red line in Figure 11 a) the Cu 3*d*

band exhibits a shift to higher energy, but its shape remains essentially unchanged, indicating no change in hybridization upon adsorption with Na. Due to the lack of covalent contribution, the difference in adsorption energy (Figure 5 in the main text) lays along the electronegativity line, and due to the electron donation from Na to the already electron-rich copper center in AgCu, the bonding is weaker on the alloy than on elemental copper. The case of Ca and the group 2 elements is similar, except that the ε_a sits below the Fermi level. This has the consequence that the broadened adsorbate states are filled to above ε_a. Localized states with energies above ε_a have anti-bonding character, and are more anti-bonding when interacting with the narrow *d*-band of AgCu than with elemental copper. This contribution from anti-bonding character makes the group 2 elements even more weakly bound to the alloy than the group 1 elements, resulting in points in Figure 5 of the main text that sit above the electronegativity line.

The $(\varepsilon-\varepsilon_a)/V^2$ lines of the group 4 adsorbates begin to intersect the Hilbert transform at two points, giving rise to splitting. The splitting is apparent in the pDOS of the C 2*p* states shown in Figure S.11 c). The areas filled with hatched lines represent bonding states, while the solid-filled areas represent anti-bonding states. The Cu 3*d* band also shows signs of hybridization, as indicated in Figure S.11 c), while some of the Cu 3*d* states (the d_{yz}, d_{xy}, and d_{xz} states) are non-bonding, as indicated by the solid red region of the pDOS. Due to the position of the Fermi level with respect to these split states, the filling of bonding and anti-bonding states does not significantly differ between adsorbates on AgCu and elemental Cu.

In Groups 5, 6 and 7 adsorbates (group 5 not shown here), there is a strong interaction between the adsorbate states and the *d*-band. For these cases, the $(\varepsilon-\varepsilon_a)/V^2$ lines intersect the Hilbert transform twice, giving rise to split adsorbate states, as shown in Figure 11 f). The split states and hybridization of the Cu 3*d* is very apparent in the pDOS's of these adsorbates shown in Figure 11 d)-e). On AgCu, due to the narrowness of the *d*-band, the anti-bonding states of the adsorbate are generally less populated than on elemental copper, giving rise to stronger bonding on the alloy than elemental copper. Fluorine is an outlier among its group. Because of its very high electronegativity, its ε_a is so far below the Fermi level that both its bonding and anti-bonding states are occupied when adsorbed to AgCu and Cu alike, and therefore its adsorbtion energy difference is due to ionic interactions only and in Figure 5 (of main text) its point sits on the electronegativity line.

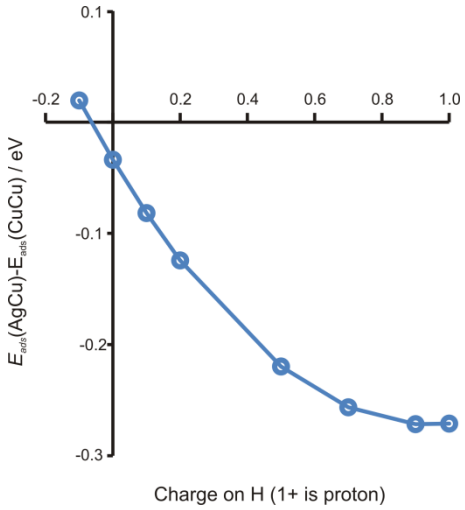

Figure 12 - Difference in adsorption energy between H adsorbed to AgCu and H adsorbed to CuCu plotted as a function of the charge on H. This plot demonstrates that the more positively charged the H ion is the more strongly it bonds to AgCu than CuCu.

In the methoxy dehydrogenation step of the methanol reforming reaction, one proton is abstracted from the methoxy group. This step involves a nucleophilic attack by the catalyst. Figure 12 shows a plot of the difference in adsorption energy between an H ion adsorbed to the Cu site of AgCu and an H ion adsorbed to a pure Cu surface. The difference in adsorption energy is plotted as a function of the charge on the H ion. The H charge was set as a tunable parameter. Here we can see that the more positively charged the H ion, the stronger it bonds to AgCu than to pure Cu. The reason for this result is that the Cu center in AgCu is negatively charged, while in pure Cu it is neutral. Therefore, due to the ionic contribution to bonding, the bond strength becomes increasingly stronger on AgCu as the positive charge on the H ion increases.